Explorations of the BSSN Formalism Under Spherical Symmetry

Hank Chen, J. Leo Kim, and Dorsa Sadat Hosseini Khajouei

ABSTRACT

Einstein's theory of general relativity remains one of the most successful theories in modern physics to date. The governing set of Einstein Field Equations (EFEs) describe the deformation of spacetime geometry around massive objects, and yields extremely accurate predictions regarding astronomical and cosmological observations. In this report on numerical relativity, we consider the Generalized Baumgarte-Shaprio-Shibata-Nakamura (GBSSN) formulation of the EFEs (Shibata & Nakamura 1995; Baumgarte & Shapiro 1999) in spherical symmetry. Following Ref. (Brown, J. David 2008), we will reproduce some of the results, then compute some important physical quantities of the spherically-symmetric blackhole. In particular, we produce computations of the expansion, event horizon, as well as the the lightcones in nearby regions.

1. INTRODUCTION

General relativity, at its core, is a *gauge theory of geometries* on a pseudo-Riemannian manifold (M, g), where g is the symmetric metric tensor. The associated Einstein Field Equations (EFEs) in natural units $G = c = 1$ read

$$\text{Ric}_{\mu\nu} - \frac{1}{2}\mathcal{R} = \begin{cases} 0 & ; \textbf{Vacuum} \\ 8\pi T_{\mu\nu} & ; \textbf{Matter} \end{cases}, \tag{1}$$

where Ric is the Ricci tensor, $\mathcal{R}$ the scalar curvature and T the stress-energy tensor. Under the assumption of spherical symmetry, it can be shown that the *unique* (up to isometry) static spherically-symmetric solution g to the vacuum EFEs is the diagonal **Schwarzschild metric**

$$g_{\mu\nu}dx^\mu dx^\nu = -\left(1 - \frac{2M}{r}\right)dt^2 + \frac{dr^2}{1 - \frac{2M}{r}} + r^2 d\Omega^2, \qquad d\Omega^2 = d\theta^2 + \sin^2\theta d\phi^2, \tag{2}$$

with $d\Omega^2$ the standard metric on the unit sphere $S^2 \subset \mathbb{R}^3$. Without symmetry assumptions, however, the EFEs are very difficult to solve, and one often must pursue numerical simulations.

By expressing the EFEs as Hamilton's equations of motion in the **ADM Hamiltonian formalism**, it allows us to leverage first-order integration schemes to compute the time derivative at each step, instead of solving for all four components of the metric g at once. However, the ADM formalism lacks long-term numerical stability. To amend this the **BSSN formalism** (Shibata & Nakamura 1995; Baumgarte & Shapiro 1999) introduces an auxiliary variable B that fixes the gauge, which stabilizes the Hamiltonian evolution. The **generalized BSSN (GBSSN) formalism** further relaxes the unimodularity det $g = 1$ condition (Brown 2005; Brown, J. David 2008).

2. THE GENERALIZED BSSN FORMALISM IN SPHERICAL SYMMETRY

Given a Schwarzschild black hole at the origin, consider a (3+1) foliation of spacetime $\Sigma \times \mathbb{R} \subset M \setminus \{0\}$ given by the punctured 3-space $\Sigma \cong \mathbb{R}^3 \setminus \{0\}$. The induced metric g on Σ induces in turn a **connection** Γ, and introduces the **extrinsic curvature** K of Σ. In terms of these quantities, the Hamiltonian, momentum and conformal constraints can be written

$$\mathcal{H} = K^2 - K^{ij}K_{ij} + \mathcal{R}, \qquad \mathcal{M}^i = \nabla_j K^{ij} - \nabla^i K, \qquad \mathcal{G}^i = \Gamma^i - g^{jk}\Gamma^i_{jk}. \tag{3}$$

Furthermore, the lapse function α and shift vector β^i satisfy the $1 + \log$ **slicing** and Γ**-driver** conditions (see Appendix), which ensure respectively the stability under time evolution of the foliation Σ and the gauge fixing by B. Introduce two normalizations: the **conformal metric** γ and the **trace-free curvature** A, defined by

$$g_{ij} = e^{4\phi}\gamma_{ij} = \chi^{-1}\gamma_{ij}, \qquad K_{ij} = \chi^{-1}\left(A_{ij} + \frac{1}{3}\gamma_{ij}K\right); \tag{4}$$

we also denote by $\Upsilon^i = \gamma^{jk}\Upsilon^i_{jk}$ the **conformal connection** built from the conformal metric γ.

Now suppose Σ is spherically symmetric, whence γ, A become diagonal. We parameterize $\Sigma \cong \mathbb{R}^3 \setminus \{0\}$ with spheres $S_r^2 \subset \mathbb{R}^3$ of radius $r > 0$. We take our ansatz to be

$$A_{ij} = A_{rr}\text{diag}\left(1, -\frac{\gamma_{\theta\theta}}{\gamma_{rr}}, -\frac{\gamma_{\theta\theta}}{\gamma_{rr}}\sin^2\theta\right), \qquad \Upsilon^i = \left(\Upsilon^r \quad -\frac{\cos\theta}{\sin\theta}\gamma_{\theta\theta} \quad 0\right). \tag{5}$$

The GBSSN formalism under spherical symmetry (Brown, J. David 2008), involving the above state variables, shall be our main focus. To explore further than the article, we shall also compute the location of the event horizon, as well as the behaviour of the lightcones near it.

3. METHODS

3.1. *Description of numerical method*

In this section, we outline the GBSSN evolution equations and the numerical methods used to solve it. The numerical part of this project is done completely in `MATLAB`, and the version control was performed using `git` via GitHub[1]. Our state variables for time evolution is composed of nine quantities $\alpha, \beta^r, B^r, \chi, \gamma_{rr}, \gamma_{\theta\theta}, A_{rr}, K, \Upsilon^r$. In the following, we denote by primes the derivatives with respect to r. For the rest of this report, we shall focus on the *Lagrangian* condition of the GBSSN equations; see Ref. (Brown, J. David 2008) and the Appendix. A further set of constraint evolution equations for the quantities in Eq. (3) are imposed, in order to ensure that the state variables stay on-shell throughout the evolution.

We use a fourth-order central finite difference scheme to compute the derivatives, similar to Brown, J. David (2008). This differs slightly from the exact scheme in the article, which uses a shifted finite difference stencil around the coordinate singularity at the origin with an additional guard cell. While normally two-level boundary conditions would be required, we instead make use of the spatial parity of our variables near the origin: we impose even parity for objects with even numbers of the index r and odd parity for objects with odd numbers of the index r. This way, for $r = 0$, we have that

---

$f(-h) = f(h)$ and $f(-2h) = f(2h)$ for even parity quantities (such as A_{rr} or χ), and $f(-h) = -f(h)$ and $f(-2h) = -f(2h)$ for odd parity quantities (such as β^r or Υ^r). At the external boundary, we assert artificial boundary conditions by computing the parameters (since they are functions of r) explicitly outside the region.

For the temporal integration scheme, we use MATLAB's built-in `ode45` library, which is an explicit Runge-Kutta (4,5) integrator (Shampine & Reichelt 1997). To do this, we require that all of our parameters are packed into one $(12N, 1)$ state vector U, where N is the number of grid points, since `ode45` requires that the input for the time evolution is given as a column vector. Since we have 9 parameters of interest to evolve, each grid points will have 9 elements in the vector assigned to it. In our set-up, the information for the first cell is captured in `U(1:9,1)`, the information for the second cell in `U(10:18, 1)`, and so on.

3.2. *Flat initial conditions*

As an intermediate test, we check to see if the right hand side of the Eqs. (A1a)-(A1i) converge to zero for a flat spacetime in spherical coordinates. The nonzero initial conditions for our flat spacetime simulation in the interval $r_{\min} = 1$ and $r_{\max} = 10$ are given by

$$\alpha(0, r) = 1, \qquad \chi(0, r) = 1, \qquad \gamma_{rr}(0, r) = 1, \qquad \gamma_{\theta\theta}(0, r) = r^2, \qquad \Upsilon^r(0, r) = -\frac{2}{r}, \quad (6)$$

while all the other parameters vanish. In general relativity, given an empty universe and a flat spacetime, we expect there to be no time evolution given any initial state. To do this, we calculate the L^2 grid norm for the right hand side at a resolution h, knowing that the actual solution would just have 0 everywhere for the time derivative.
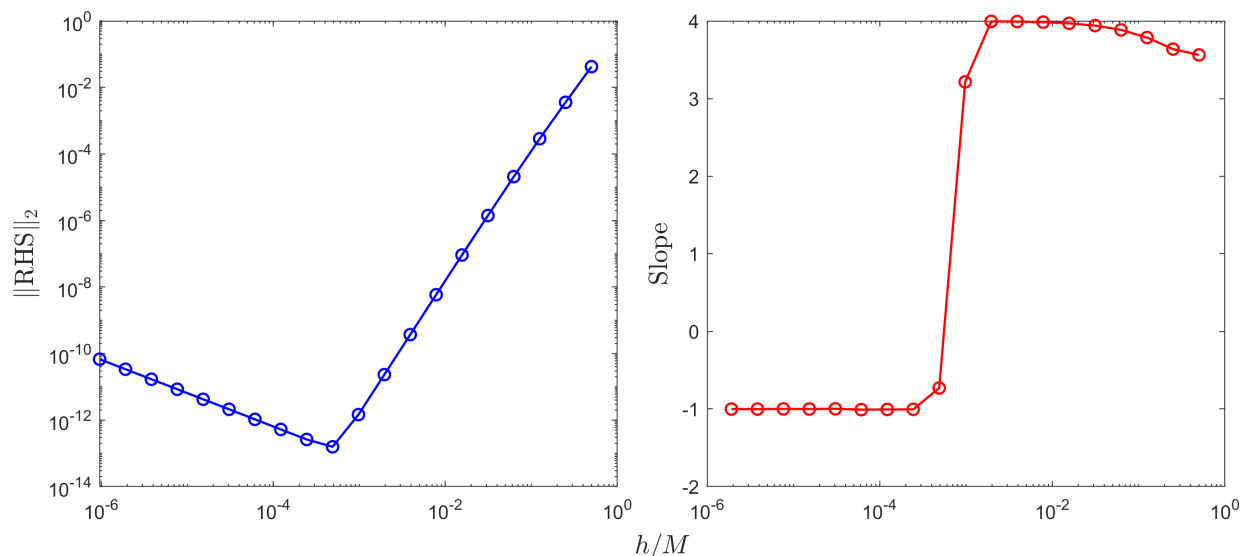
Figure 1. Convergence of RHS of Eqs. (A1a)-(A1i). The left plot gives the log-log plot of the L^2 grid norm of the entire right hand side equations, while the right plot gives the slope of the left plot on a semi-log scale.

The computation of the L^2 grid norm for the right hand side of equations (A1a)-(A1i) is shown in figure 1. As expected, we see fourth order convergence of the right hand side to 0 in between the regions $h \sim 10^{-1}$ to $h \sim 10^{-3}$. For finer resolutions, we expect that floating point error dominates.

3.3. *Puncture initial conditions*

To capture the initial conditions for blackhole evolution, we use the puncture initial conditions (Brandt & Seidel 1995; Cook 2000). For puncture evolution in spherical symmetry, we take the Schwarzschild metric Eq. (2) induced on Σ (without the dt^2 term) as the initial condition of the metric $g = \chi^{-1}\gamma$. The non-zero components of our problem are then

$$\alpha(0,r) = \left(1 + \frac{2M}{r}\right)^{-2}, \quad \chi(0,r) = \left(1 + \frac{2M}{r}\right)^{-4}, \quad \gamma_{rr}(0,r) = 1, \quad \gamma_{\theta\theta}(0,r) = r^2, \quad \Upsilon^r(0,r) = -\frac{2}{r},$$

$$(7)$$

while the rest of the remaining parameters are vanishing initially. Note that the initial form of α is the "pre-collapsed" form of α. This form of the initial condition for α is more stable than the unit α initial condition, which approaches the pre-collapsed form when evolved in time, except at $r = 0$.
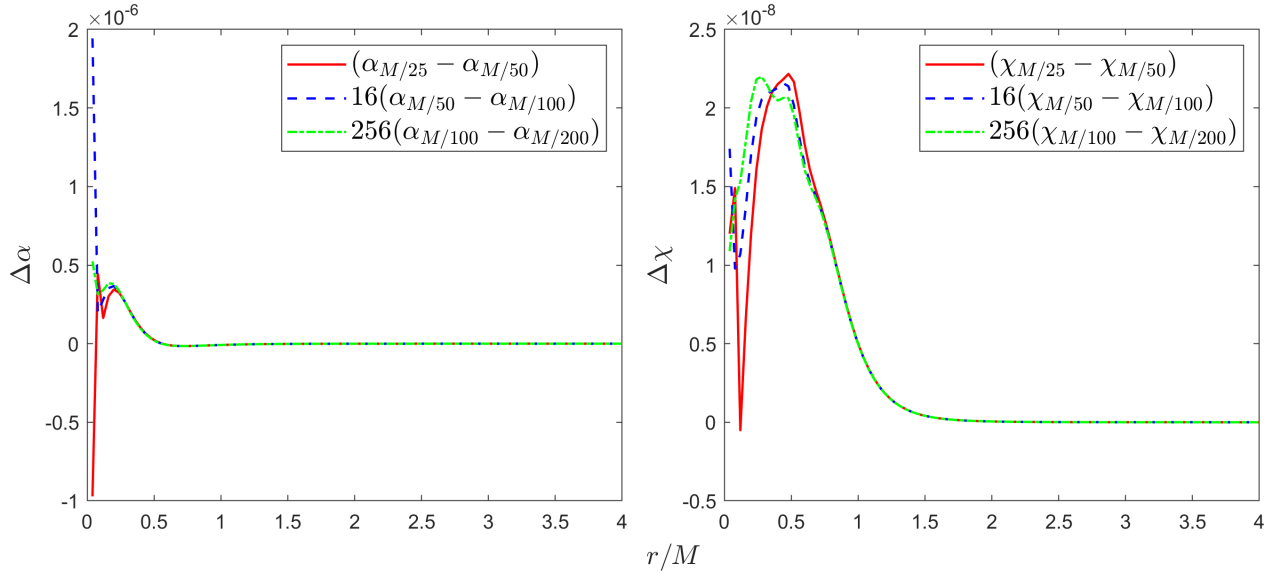
Figure 2. Convergence of $\Delta\alpha$ and $\Delta\chi$ at $t = 0.5M$. The finer differences (dashed lines) are scaled by powers of 16 for comparison at the fourth-order convergence level.

Figures 2 and 3 shows the pointwise convergence for $\Delta\alpha$ and $\Delta\chi$, where we calculate the pointwise difference between α and χ at two different resolutions, then scale them by factors of 16 for the desired fourth-order convergence. Since we compute the pointwise difference between these points, the differences are taken at every $M/25$.

We observe that while the convergence plots agree as r increases, the puncture initial condition at $r \sim 0$ results in instabilities due to the coordinate singularity at the origin in spherical coordinates. Terms in the system such as $\Upsilon^r(0,r) \sim -2/r$ or $1/\gamma_{\theta\theta} \sim 1/r^2$ lead to large errors near the origin. While $\Delta\alpha$ seems to show convergence at fourth-order, $\Delta\chi$ appears to show propagation of error at the boundary $r = 0$. Due to the coordinate singularity as well as the imperfect boundary conditions, this makes sense, although it is not a problem from a physical perspective, since most of the numerical instability is captured in the event horizon of the blackhole, which is the system's barrier for information transfer. Lastly, $r_{\max}$ for these simulations were done at $r \sim 10M$, due to
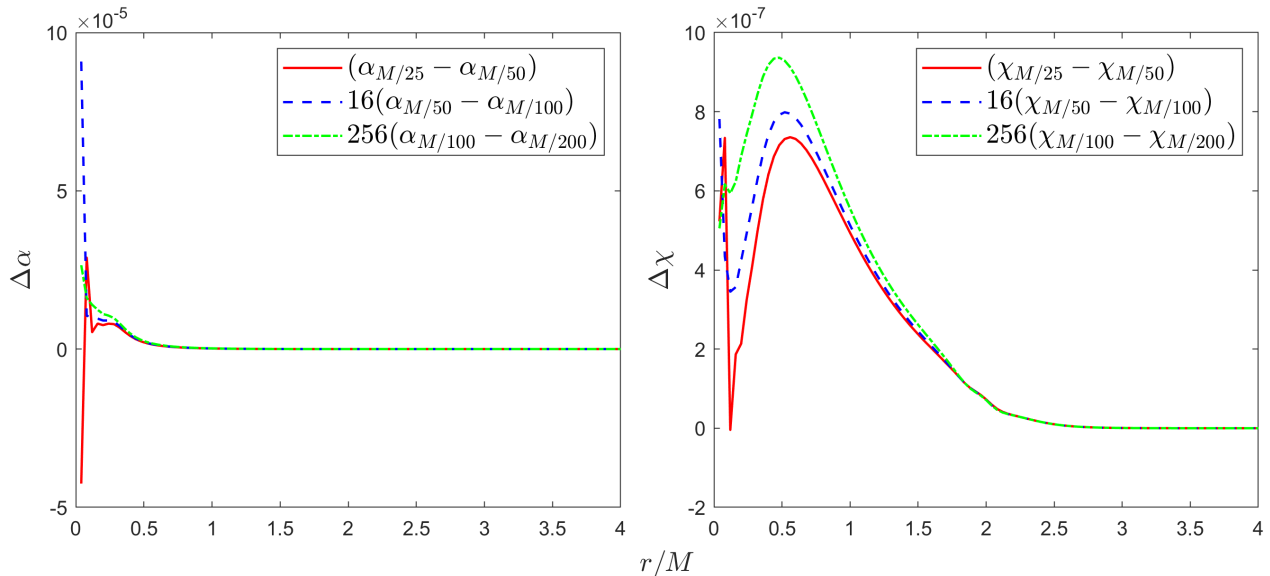
Figure 3. Convergence of $\Delta\alpha$ and $\Delta\chi$ at $t = 2M$. The finer differences (dashed lines) are scaled by powers of 16 for comparison at the fourth-order convergence level.

the fact that instabilities can also propagate inwards from the outer boundary. By selecting a large enough $r_{\max}$ for the simulation and a small enough r for the pointwise convergence calculation, we can take snapshots of the convergence before instabilities propagate into our calculations from the outer boundary.

4. RESULTS

In this section we will outline the main results of the project. Section 4.1 is still in line with the article (Brown, J. David 2008), where we discuss the convergence of the constraints under our numerical scheme. However in sections 4.2 and 4.3, we investigate beyond the contents of Brown (2005) and compute some physical quantities of interest, such as the expansion and horizon of a black hole, as well as the lightcones.
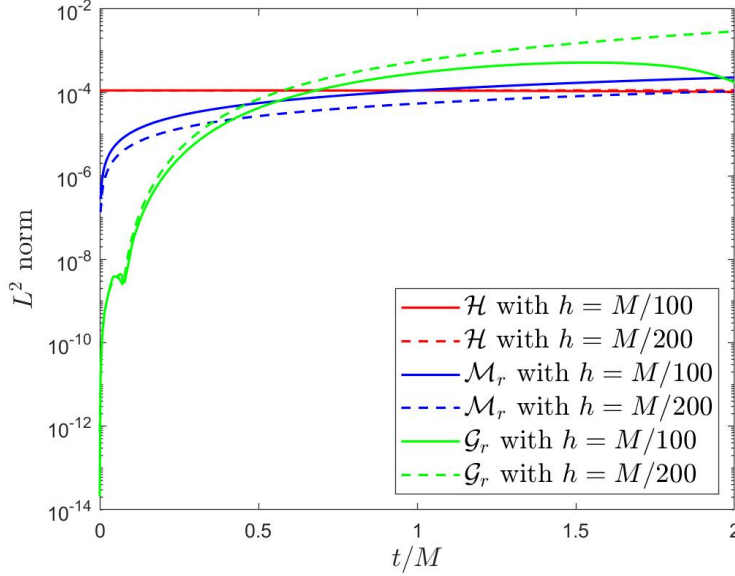
4.1. *Constraints*

Recall that the spatial metric g_{ij} is obtained from restricting the spacetime metric. One may then ask if g_{ij}, under Hamiltonian time-evolution, remains the metric which describes the spacetime geometry of Σ at later times. This is of course not in general the case, but the constraints Eq. (3) are imposed precisely to enforce this. In other words, the quantities $\mathcal{H}, \mathcal{M}^r, \mathcal{G}^r$ must all identically vanish throughout each time-step in order to ensure that the state variables remain **on-shell**, i.e. solutions of the EFEs.

Now instead of enforcing the constraints to vanish by hand in each time-step, we may evolve these constraints along with time such that the state variables stay on-shell, *given* the constraint eovlution equations are imposed. In the spherically-symmetric GBSSN formalism, these equations are given in Ref. Brown, J. David (2008) and the Appendix.

In principle, as we have taken a Schwarzschild-like on-shell initial condition Eq. (7), the constraints are by definition zero at $t = 0$. As the state variables evolve according to Eqs. (A1a)-(A1i), these

constraints are only guaranteed to vanish up to the finite-differencing error. As such, we expect a fourth-order convergence to zero for the constraints Eq. (3) at late times $t > 0$.

Figure 4. Convergence of the L^2-grid norms for the constraints $\mathcal{H}, \mathcal{M}^r, \mathcal{G}^r$ on a grid $r_{\min} = M/25$ to $r_{\max} = 10M$. The dashed lines are computed at the finer resolution $N = 200$, while the solid lines are computed at the coarser resolution $N = 100$. The dashes lines are scaled by 16 for fourth-order convergence.

In order to test the "on-shell-ness" of our numerical implementation, we compute the L^2-grid norms of $\mathcal{H}, \mathcal{M}^r, \mathcal{G}^r$ as they evolve according to Eqs. (B3a)-(B3c). These are shown in Fig. 4, where the Hamiltonian $\mathcal{H}$ as well as the momentum $\mathcal{M}^r$ constraints expectedly converge at fourth-order. The conformal constraint $\mathcal{G}^r$, on the other hand, has a hard time converging. We suspect that this is due to the coordinate singularity in the conformal connection Υ^r (see Eq. (7)), and hence creates numerical artifacts and oscillations that violate the constraint condition.

4.2. *Expansion and event horizon*

A particular quantity of physical interest is the **expansion parameter** (Thornburg 2007)

$$\Theta = \nabla_i n^i + K_{ij} n^i n^j - K, \tag{8}$$

where n is a unit normal vector to the 3-space foliation Σ. A closed compact embedded 2-surface $\Lambda \subset \Sigma$ has $\Theta|_\Lambda = 0$ iff $K = \nabla_i n^i$ and $K_{ij} n^i n^j = 0$, hence it is locally flat with trivial extrinsic curvature. Λ is called a marginally outer trapped surface, or the **(event) horizon**, between which the curvature of spacetime changes character. It is an important quantity that detects the onset of the formation of a blackhole.

With spherical symmetry of Σ, we may write

$$\Theta = \frac{g'_{\theta\theta}}{g_{\theta\theta}\sqrt{g_{rr}}} - 2\frac{K_{\theta\theta}}{g_{\theta\theta}} \tag{9}$$

in terms of the physical metric g_{ij} and extrinsic curvature K_{ij}. Recall the conformal metric $g_{ij} = \chi^{-1}\gamma_{ij}$ and that $K_{\theta\theta}$ can be written in terms of $A_{\theta\theta} = -A_{rr}\frac{g_{\theta\theta}}{2g_{rr}}$ and its trace K, the expansion

$\Theta = \Theta(\gamma_{rr}, \gamma_{\theta\theta}, \chi, A_{rr}, K)$ can be computed in terms of the state variables in Eqs. (A1a)-(A1i). By bracketing the root

$$\Theta = \Theta(t, r = r_{\text{hor}}(t)) = 0, \tag{10}$$

we obtain the horizon radius $r_{\text{hor}}(t)$ at each time t. This is accomplished by a simple root-finding algorithm, in which the sign of the multiple of successive values of Θ are tested across the spatial grid $r = (0, r_1, \ldots, r_N)$. If $i < N$ is such that $\Theta(r_i)\Theta(r_{i+1}) < 0$, then the horizon is obtained as a linear $r_{\text{hor}} = \frac{1}{2}(r_i + r_{i+1})$ interpolation.

The time evolution of the expansion Θ, as well as the horizon radius r_{hor}, obtained from our numerical computations are shown in Fig. 5 below.
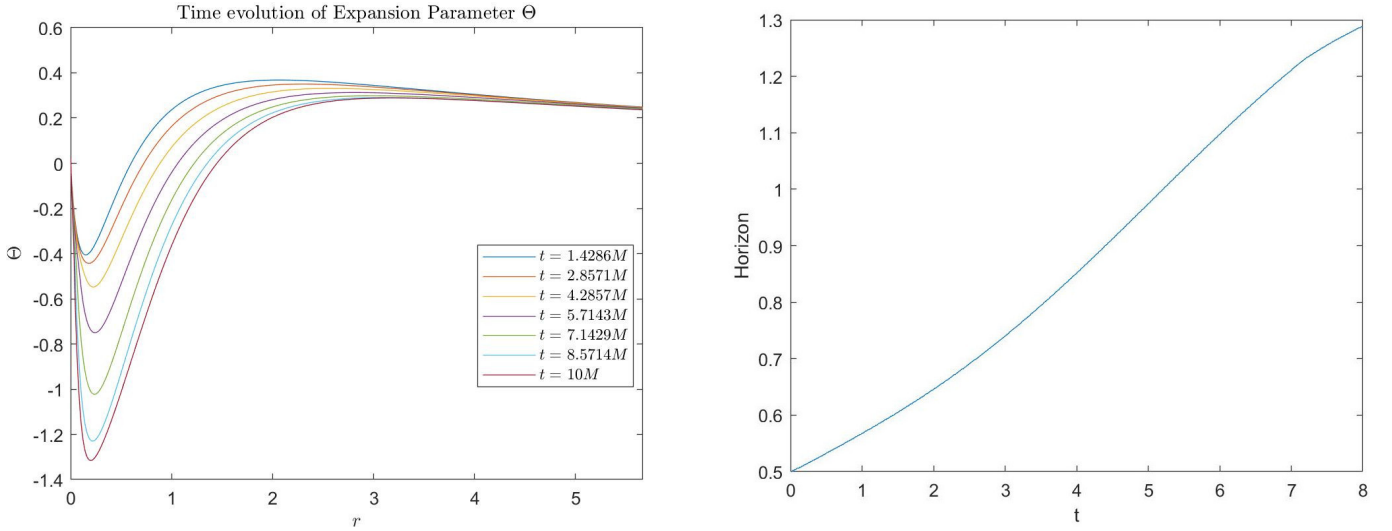
Figure 5. The expansion parameter $\Theta = \Theta(t, r)$ for $0 < t < 5M$, plotted at selected partitions of time in unites of $t/7$, and the time evolution of the horizon radius $r_{\text{hor}} = r_{\text{hor}}(t)$ up to $t = 8M$. Here, the spatial grid in the expansion plot has $r_{\max} = 17$ and resolution has $N = 200$. For the horizon plot, on the other hand, we take a higher resolution $N = 500$ in order to stabilize the root-finder.

It can be seen that, for each t, the expansion achieves a global minimum and asymptotes to a steady value $\lesssim 0.4$. Furthermore, the horizon grows approximately linearly in time from $r_{\text{hor}}(0) = \frac{1}{2}$, hinting at the expansion of the blackhole horizon.

Once the horizon r_{hor} has been obtained, we may obtain the **Misner-Sharp** blackhole mass, which for a Schwarzschild solution Eq. (2) reads $2M = r_{\text{hor}}$ (Nielsen & Yeom 2009). This is a subtle relation that holds only at the horizon, however, and M is in fact time independent.

4.3. *Lightcones*

An alternative signal for the formation of a blackhole is the lightcones. These are regions in M spanned by null-vectors u, for which $|u|^2 = g_{\mu\nu}u^\mu u^\nu = 0$. In spherical symmetry, this gives the equation

$$0 = \left(-\frac{\alpha^2}{g_{rr}} + (\beta^r)^2\right)(u^t)^2 + 2\beta^r u^t u^r + (u^r)^2. \tag{11}$$

Without loss of generality, taking $u^\mu = (u^t = 1, u^r, 0, 0)$ leads to the solutions

$$u^r = u^r_\pm(t, r) = -\beta^r \pm \sqrt{\frac{\alpha^2}{\chi^{-1}\gamma_{rr}}}. \tag{12}$$

Far away from the blackhole singularity, spacetime is by hypothesis flat, hence the lightcones are upright. However, as r is tuned towards the horizon radius, the lightcones begin to tilt towards the blackhole singularity. If the tilting is severe enough to trap the null vectors, then an **apparent horizon** forms at the horizon radius $r = r_{\text{hor}}$ when $u^r_+ = 0$. We can also get a more concrete idea of how the lightcones evolve with the **normalized lightcone deficit angle** θ_0, satisfying

$$\tan\frac{\pi}{4}\theta_0 = u^r_+. \tag{13}$$

Locations at which $\theta_0 \leq 0$ indicate trapped surfaces.
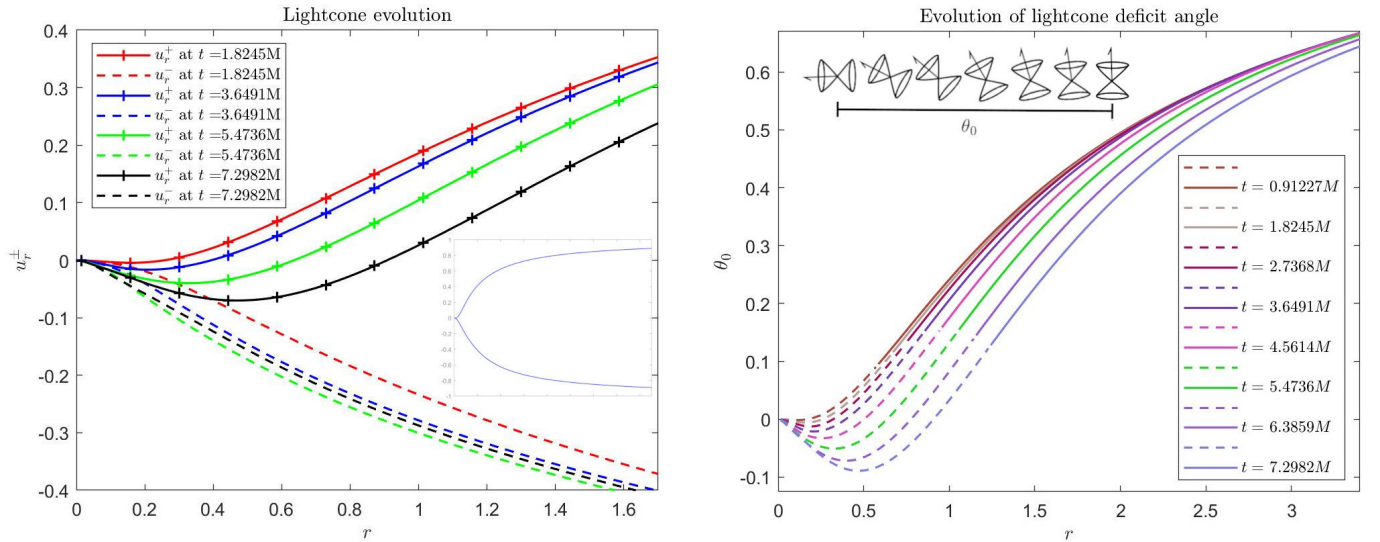
Figure 6. Lightcone plots as a function of r for times up to $t = 7.3M$, plotted at selected partitions of time in units of $2 \times t/8$. The maximal radius is $r_{\text{max}} = 17$, and the resolution is taken to be $N = 70$. **Left**: The null vectors $u^r_\pm$; the inset shows the large-r behaviour $u^r_\pm \approx \pm 1$. **Right**: The normalized deficit angle θ_0 defined by Eq. (13), with asymptotic behaviour $\theta_0 \approx 1$ at $r \gg r_{\text{hor}}$. The solid/dashed lines represent the deficit angles without/within the horizon, respectively.

Our numerical simulations of the lightcone data $u^r_\pm, \theta_0$ are shown in Fig. 6. First, notice that $u^r_\pm \to \pm 1$ and $\theta_0 \to 1$ as $r \to \infty$, which implies that the lightcones are indeed upright (at 90-degrees with the spatial slice Σ) asymptotically away from the horizon. Furthermore, for sufficiently large times $t \gtrsim 2M$ such that the null vectors stabilize, one may also see by comparing with Fig. 5 that positive roots of $u^r_+ = 0$ occur approximately at the horizon $r = r_{\text{hor}}$.

Near the horizon, we also see an obvious tilting of the lightcones shown by the decreasing θ_0 as $r \to 0^+$ approaches the blackhole singularity from the right. Once again for sufficiently large times $t \gtrsim 2M$, the locations r at which $\theta_0 \lesssim 0$ becomes negative can be seen to coincide approximately with the horizon r_{hor} by comparison with Fig. 5. Within the blackhole, the deficit angle $\theta_0 < 0$, which signals to the fact that lightrays can in fact only propagate *into* the blackhole singularity.

5. CONCLUSION

In this review, following Brown, J. David (2008), we have explored the GBSSN formalism of general relativity, which is the re-formulation of the standard BSSN formalism under spherical symmetry. Using a fourth order finite difference scheme, we reproduced the results of the paper and checked convergence for the numerical schemes and constraints under flat and puncuture initial conditions. Going beyond the paper, we also computed several physically significant quantities, such as the expansion and event horizon of a black hole, as well as the tilting of the lightcones for spacelike observers. The GBSSN equations prove to be a powerful numerical formulation for looking at spherically symmetric systems and their physically important quantities.

ACKNOWLEDGEMENTS

APPENDIX

A. THE GBSSN EQUATIONS

Recall derivatives with respect to r are denoted by primes, the GBSSN equations are given by (Brown, J. David (2008)):

$$\partial_t \alpha = \beta^r \alpha' - 2\alpha K \ , \tag{A1a}$$

$$\partial_t \beta^r = \frac{3}{4} B^r + \beta^r \beta^{r'} \ , \tag{A1b}$$

$$\partial_t B^r = \partial_t \Upsilon^r + \beta^r B^{r'} - \beta^r \Upsilon^{r'} - \eta B^r \ , \tag{A1c}$$

$$\partial_t \chi = \frac{2K\alpha\chi}{3} - \frac{v\beta^r \gamma_{rr}'\chi}{3\gamma_{rr}} - \frac{2v\beta^r \gamma_{\theta\theta}'\chi}{3\gamma_{\theta\theta}} - \frac{2}{3}v\beta^{r'}\chi + \beta^r \chi' \ , \tag{A1d}$$

$$\partial_t g_{rr} = -2A_{rr}\alpha - \frac{1}{3}v\beta^r \gamma_{rr}' + \beta^r \gamma_{rr}' - \frac{2\gamma_{rr}v\beta^r \gamma_{\theta\theta}'}{3\gamma_{\theta\theta}} + 2\gamma_{rr}\beta^{r'} - \frac{2}{3}\gamma_{rr}v\beta^{r'} \ , \tag{A1e}$$

$$\partial_t g_{\theta\theta} = \frac{A_{rr}\gamma_{\theta\theta}\alpha}{\gamma_{rr}} - \frac{\gamma_{\theta\theta}v\beta^r \gamma_{rr}'}{3\gamma_{rr}} - \frac{2}{3}v\beta^r \gamma_{\theta\theta}' + \beta^r \gamma_{\theta\theta}' - \frac{2}{3}\gamma_{\theta\theta}v\beta^{r'} \ , \tag{A1f}$$

$$\partial_t A_{rr} = -\frac{2\alpha A_{rr}^2}{\gamma_{rr}} + K\alpha A_{rr} - \frac{v\beta^r \gamma_{rr}'A_{rr}}{3\gamma_{rr}} - \frac{2v\beta^r \gamma_{\theta\theta}'A_{rr}}{3\gamma_{\theta\theta}} - \frac{2}{3}v\beta^{r'}A_{rr} + 2\beta^{r'}A_{rr} + \frac{2\alpha\chi\left(\gamma_{rr}'\right)^2}{3\gamma_{rr}^2}$$
$$- \frac{\alpha\chi\left(\gamma_{\theta\theta}'\right)^2}{3\gamma_{\theta\theta}^2} - \frac{\alpha\left(\chi'\right)^2}{6\chi} - \frac{2\gamma_{rr}\alpha\chi}{3\gamma_{\theta\theta}} + \beta^r A_{rr}' + \frac{2}{3}\gamma_{rr}\alpha\chi\Upsilon^{r'} - \frac{\alpha\chi\gamma_{rr}'\gamma_{\theta\theta}'}{2\gamma_{rr}\gamma_{\theta\theta}} + \frac{\chi\gamma_{rr}'\alpha'}{3\gamma_{rr}}$$
$$+ \frac{\chi\gamma_{\theta\theta}'\alpha'}{3\gamma_{\theta\theta}} - \frac{\alpha\gamma_{rr}'\chi'}{6\gamma_{rr}} - \frac{\alpha\gamma_{\theta\theta}'\chi'}{6\gamma_{\theta\theta}} - \frac{2\alpha'\chi'}{3} - \frac{\alpha\chi\gamma_{rr}''}{3\gamma_{rr}} + \frac{\alpha\chi\gamma_{\theta\theta}''}{3\gamma_{\theta\theta}} - \frac{2\chi\alpha''}{3} + \frac{\alpha\chi''}{3} \ , \tag{A1g}$$

$$\partial_t K = \frac{3\alpha A_{rr}^2}{2\gamma_{rr}^2} + \frac{K^2\alpha}{3} + \beta^r K' + \frac{\chi\gamma_{rr}'\alpha'}{2\gamma_{rr}^2} - \frac{\chi\gamma_{\theta\theta}'\alpha'}{\gamma_{rr}\gamma_{\theta\theta}} + \frac{\alpha'\chi'}{2\gamma_{rr}} - \frac{\chi\alpha''}{\gamma_{rr}} \ , \tag{A1h}$$

$$\partial_t \Upsilon^r = -\frac{v\beta^r \left(\gamma_{\theta\theta}'\right)^2}{\gamma_{rr}\gamma_{\theta\theta}^2} + \frac{A_{rr}\alpha\gamma_{\theta\theta}'}{\gamma_{rr}^2\gamma_{\theta\theta}} - \frac{v\beta^{r'}\gamma_{\theta\theta}'}{3\gamma_{rr}\gamma_{\theta\theta}} + \frac{\beta^{r'}\gamma_{\theta\theta}'}{\gamma_{rr}\gamma_{\theta\theta}} + \beta^r \Upsilon^{r'} + \frac{A_{rr}\alpha\gamma_{rr}'}{\gamma_{rr}^3} - \frac{4\alpha K'}{3\gamma_{rr}} - \frac{2A_{rr}\alpha'}{\gamma_{rr}^2}$$
$$+ \frac{v\gamma_{rr}'\beta^{r'}}{2\gamma_{rr}^2} - \frac{\gamma_{rr}'\beta^{r'}}{2\gamma_{rr}^2} - \frac{3A_{rr}\alpha\chi'}{\gamma_{rr}^2\chi} + \frac{v\beta^r \gamma_{rr}''}{6\gamma_{rr}^2} + \frac{v\beta^r \gamma_{\theta\theta}''}{3\gamma_{rr}\gamma_{\theta\theta}} + \frac{v\beta^{r''}}{3\gamma_{rr}} + \frac{\beta^{r''}}{\gamma_{rr}} \ , \tag{A1i}$$

where the parameter v acts as a switch for the Eulerian ($v = 0$) or the Lagrangian ($v = 1$) condition, and B is the gauge-fixing auxiliary variable in the BSSN formalism.

LAGRANGIAN AND EULERIAN CONSTRAINTS

Let us introduce the "foliated Killing vector" $\partial_\perp = \partial_t - \mathcal{L}_\beta$, where $\mathcal{L}_\beta$ is the Lie derivative along the shift vector β. In the GBSSN formalism, we have a (gauge) freedom in choosing how the quantity $\mathfrak{g} \equiv \ln g$ evolves along $\partial_\perp$. Given the foliated time evolution $\partial_\perp$, there are two natural choices

$$\textbf{Eulerian}: \quad \partial_\perp \mathfrak{g} = 0, \qquad \textbf{Lagrangian}: \quad \partial_t \mathfrak{g} = 0. \tag{A2}$$

These conditions mean that the characteristic field φ introduced by the determinant $\mathfrak{g}$ has vanishing speed on Σ under the Eulerian condition, while it depends on the shift vector β under the Lagrangian condition. As such this speed becomes a quantity whose time-evolution is gauge non-invariant. This does not pose a problem in terms of numerical implementation, as one may just ignore such a field φ, as long as the constraints are imposed consistently at each time-step.

B. THE CONSTRAINT EVOLUTION EQUATIONS

The Hamiltonian $\mathcal{H}$, momentum $\mathcal{M}^r$ and conformal $\mathcal{G}^r$ constraints Eqs. (3) satisfy the following constraint evolution equation (Brown, J. David (2008))

$$\mathcal{H} = -\frac{3A_{rr}^2}{2\gamma_{rr}^2} + \frac{2K^2}{3} - \frac{5\chi'^2}{2\chi\gamma_{rr}} + \frac{2\chi''}{\gamma_{rr}} + \frac{2\chi}{\gamma_{\theta\theta}} - \frac{2\chi\gamma_{\theta\theta}''}{\gamma_{rr}\gamma_{\theta\theta}} + \frac{2\chi'\gamma_{\theta\theta}'}{\gamma_{rr}\gamma_{\theta\theta}} + \frac{\chi\gamma_{rr}'\gamma_{\theta\theta}'}{\gamma_{rr}^2\gamma_{\theta\theta}}$$
$$- \frac{\chi'\gamma_{rr}'}{\gamma_{rr}^2} + \frac{\chi\gamma_{\theta\theta}'^2}{2\gamma_{rr}\gamma_{\theta\theta}^2}, \tag{B3a}$$

$$\mathcal{M}_r = \frac{A_{rr}'}{\gamma_{rr}} - \frac{2K'}{3} - \frac{3A_{rr}\chi'}{2\chi\gamma_{rr}} + \frac{3A_{rr}\gamma_{\theta\theta}'}{2\gamma_{rr}\gamma_{\theta\theta}} - \frac{A_{rr}\gamma_{rr}'}{\gamma_{rr}^2}, \tag{B3b}$$

$$\mathcal{G}^r = -\frac{\gamma_{rr}'}{2\gamma_{rr}^2} + \Upsilon^r + \frac{\gamma_{\theta\theta}'}{\gamma_{rr}\gamma_{\theta\theta}}. \tag{B3c}$$

Recall that these are imposed in order to ensure that the state variables remain on-shell throughout the Hamiltonian time evolution.

REFERENCES

Baumgarte, T. W., & Shapiro, S. L. 1999, Phys. Rev. D, 59, 024007, doi: 10.1103/PhysRevD.59.024007

Brandt, S. R., & Seidel, E. 1995, Phys. Rev. D, 52, 856, doi: 10.1103/PhysRevD.52.856

Brown, J. D. 2005, Phys. Rev. D, 71, 104011, doi: 10.1103/PhysRevD.71.104011

Brown, J. David. 2008, Class. Quant. Grav., 25, 205004, doi: 10.1088/0264-9381/25/20/205004

Cook, G. B. 2000, Living Rev. Rel., 3, 5, doi: 10.12942/lrr-2000-5

Nielsen, A. B., & Yeom, D.-H. 2009, International Journal of Modern Physics A, 24, 5261–5285, doi: 10.1142/s0217751x09045984

Shampine, L. F., & Reichelt, M. W. 1997, SIAM Journal on Scientific Computing, 18, 1, doi: 10.1137/s1064827594276424

Shibata, M., & Nakamura, T. 1995, Phys. Rev. D, 52, 5428, doi: 10.1103/PhysRevD.52.5428

Thornburg, J. 2007, Living Rev. Rel., 10, 3. https://arxiv.org/abs/gr-qc/0512169